Petrology, Vol. 11, No. 2, 2003, pp. 114–129. Translated from Petrologiya, Vol. 11, No. 2, 2003, pp. 128–144.

Ultramylonites and Their Significance for the Understanding of the History of the Vredefort Impact Structure, South Africa

L. L. Perchuk*, **, L. V. Sazonova*, D. D. van Reenen*, and T. V. Gerya****

** Faculty of Geology, Moscow State University, Vorob'evy gory, Moscow, 119899 Russia*
e-mail: llp@geol.msu.ru

*** Institute of Experimental Mineralogy, Russian Academy of Sciences, Chernogolovka, Moscow oblast, 142432 Russia*
e-mail: llp@iem.ac.ru

**** Department of Geology, Rand Afrikaans University,*
Auckland Park, Johannesburg, P.O. Box 524, Republic of South Africa, 2006
e-mail: ddvr@limpopo.rau.ac.za

Received July 1, 2002

Abstract—The Vredefort crater is well known in the geological literature, because it is situated in the Witwatersrand Group, the repository of almost half of the world's gold reserves, and was generated by an explosion process. One of the key problems in the history of the crater is the timing of formation of cordierite–orthopyroxene reaction structures, which develop extensively around relict garnet in the metapelites of the granulite core of the impact structure. In the middle 1970s, W. Schreyer and K. Abraham discovered a unique pseudotachylite (ultramylonite) cutting cordierite–orthopyroxene symplectites in the metapelites of the granulite core of the crater. They argued on the basis of that discovery that the symplectites were formed long before (~3 Ga) the explosion (~2 Ga) and only reequilibrated subsequently. This idea has served for many years as a starting point for many geodynamic models of the formation of the crater core. However, up to the present time, the ultramylonites cutting symplectites were never described in detail. This paper presents (1) the analysis of microscopic textural relationships between symplectites and ultramylonites, (2) the results of detailed microprobe investigations of minerals from these structures, and (3) the comprehensive mechanism of ultramylonite formation and proof for the continuous decrease of *P–T* parameters at the final stage of upheaval of the "central uplift" of the Vredefort crater. This evidence is aimed at completing the discussion of many years on the nature of the core of the Vredefort crater.

INTRODUCTION

The Vredefort impact structure (crater) was formed ca. 2 Ga ago in the Witwatersrand greenstone belt (Kaapvaal craton, southern Africa), which comprises almost half of the world's gold reserves. This crater was first studied in the second half of the XIX century by Stow (1879), who conjectured that the metamorphism of its central part was related to some magmatic (volcanic) center. Because of its radial metamorphic zoning, the Vredefort was regarded as a dome structure in the Kaapvaal craton (e.g., Ramberg, 1985). The nature of the crater's granulite core has long been the subject of heated debate. Many researchers revived the idea of Stow (1879) on the fundamental role of deep magmatic activity in the nature of metamorphism in the central part of the dome. This idea was accepted by some modern researchers (e.g., Stevens *et al.*, 1997; Gibson *et al.*, 1998), who surmised that the metamorphism of the Vredefort had been directly related to the emplacement and development of the Bushveld massif (~2.06 Ga).

One of the major problems in metamorphic history is the timing of formation of undeformed cordierite–orthopyroxene symplectites and hypersthene rims in reaction structures, which are common around relict garnet in the metapelites of the granulite core of the crater. Schreyer and Abraham (1978) and Schreyer (1983) discovered a stringer of undeformed "pseudotachylite" cutting symplectite in these rocks. Martini (1992) pointed out that the metamorphic history of the dome cannot be considered ignoring the occurrence of stishovite and coesite in the pseudotachylite of the Vredefort, especially because pseudotachylite was documented not only in the dome core but also in its framing in the lower part of the section of the Witwatersrand Group (e.g., Gibson *et al.*, 1997). Stevens *et al.* (1997) demonstrated that symplectite formation in the pseudotachylite was connected with an explosion and occurred at the final stage of postimpact metamorphism. Note that Stevens *et al.* (1997) provided a comprehensive petrographic description of the retrograde stage of postimpact metamorphism, but the derivation of the *P–T* path and dynamics of the core of the Vredefort dome was disputable (Stevens *et al.*, 1997; Gibson and Stevens, 1998). The critical analysis of their approach was given in our previous publication (Perchuk *et al.*, 2002). However, these authors discarded this path in recent publications (Gibson and Reimold, 2001; Gibson, 2002).

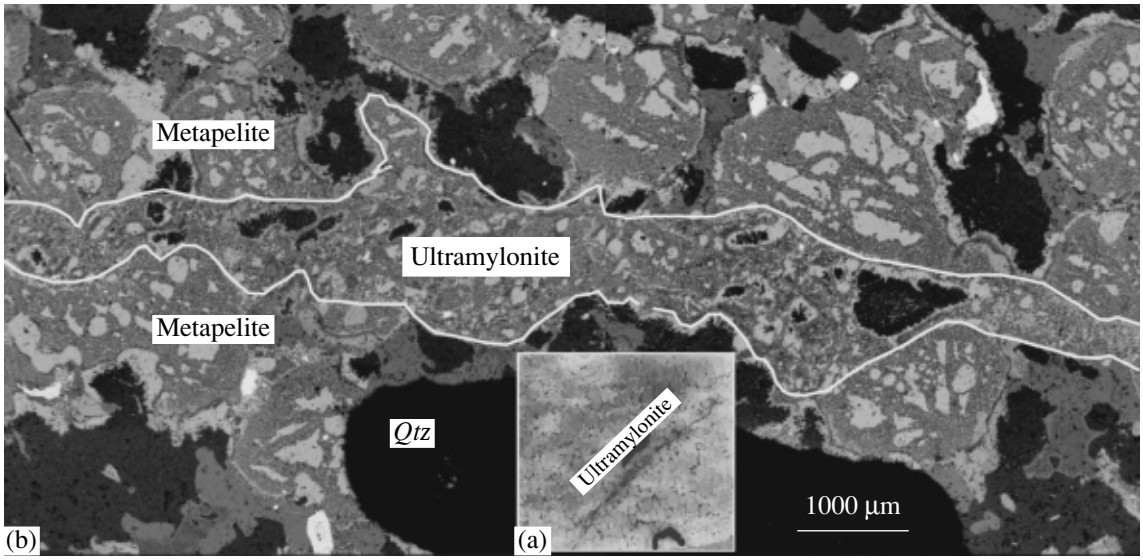

Fig. 1. Ultramylonite "veinlet" in metapelite from the core of the Vredefort impact structure.
(a) Photomicrograph of a thin section showing ultramylonite in metapelite. Transmitted light, the thin section is 20×20 mm in size.
(b) Back-scattered electron image of ultramylonite cutting metapelite. Garnet relicts are clearly seen; *Crd* + *Opx* symplectites form after them and are surrounded by orthopyroxene coronas. Rare garnet relicts in ultramylonite are enclosed by similar reaction structures. The boundary of ultramylonite is marked by the white line for clarity.

Some remarks on the terminology are necessary. Shand (1916) coined the term pseudotachylite for the dark aphanitic rocks of the Vredefort, which formed veins and glasslike veinlets. He believed that the pseudotachylites had been formed as products of melting at explosion loading. It was also speculated that friction melting is the exclusive privilege of the pseudotachylite (Allen, 1979). However, *pseudotachylite* proper is now defined as a clastic breccia of any size whose matrix shows a glassy texture (or crystallized from glass). A breccia with a clastic matrix is classified as *ultramylonite* (Wise *et al.*, 1984). The formation of these textures (rocks) results from shear stresses and accompanying plastic deformations. Both pseudotachylites and ultramylonites are formed in situ at shattering, grinding, or friction melting of rocks (Sazonova and Korotaeva, 1995) without any significant movement of the deformed material within the parental rock. Shear stresses, which eventually lead to the formation of pseudotachylites and ultramylonites, are caused by tectonic or explosion processes. Such objects in granulites are usually related to the relaxation of residual stresses due to cooling of granulite complexes in the course of their floating toward the surface (Korzhinskii, 1999). The major mechanism of this process is the gravitational redistribution of rocks within greenstone belts under the influence of fluid–heat flows (Perchuk and Gerya, 2003; Perchuk, 1989; Perchuk *et al.*, 1992).

According to the published descriptions (e.g., Schreyer and Abraham, 1978), pseudotachylite veinlets from the Vredefort metapelite do not contain glass. In accordance with the modern classification (Wise *et al.*, 1984), these thin (Fig. 1a) viscoelastic deformation features must be regarded as ultramylonites formed through the relaxation of residual stresses (Perchuk *et al.*, 2002). However, such an interpretation requires that they were formed through solid-phase transformations rather than glass (melt) crystallization. In other words, it is necessary to find out whether these veinlets were magmatic or dynamometamorphic. For this purpose, their *P–T* generation parameters must be determined. Depending on whether these parameters lie below or above the granite solidus, which is the minimum temperature of melting of any rock, the objects considered would be *ultramylonites* or *pseudotachylites*, respectively.

Remind that symplectites in the metapelite postdated the pseudotachylites and neither of them was deformed. How long was the time gap between symplectite and pseudotachylite formation? Schreyer and Abraham (1978) supposed that the symplectites were formed in the course of regional granulite metamorphism at a pressure of no less than 5 kbar. They were only reequilibrated after the explosion. Let us dismiss the attractive idea of a connection between the regional granulite-facies metamorphism of the dome core and the development of the Bushveld massif (Stevens *et al.*, 1997), because of the absence of any geochronological support (see also Gibson, 2002; Gibson and Reimold, 2001, p. 90). According to Hart (1999), the Vredefort granulites were affected by regional metamorphism more than 3 Ga ago. However, the development of the impact structure and accompanying metamorphic phenomena including the formation of pseudotachylites, symplectites, and ultramylonites occurred no earlier

than 2.023 Ga ago (Armstrong *et al.*, 1991). Thus, these two processes were separated by about a billion years! As a result, the idea of the connection of regional metamorphism in the core of the Vredefort dome with the development of the Bushveld intrusive complex was discarded (Perchuk *et al.*, 2002; Gibson, 2002; Gibson and Reimold, 2001, p. 90).

It is interesting that, irrespective of the duration of the gap, the concept of mineral reequilibration in the symplectites (Schreyer and Abraham, 1978) at a pressure of ~5 kbar has long been the starting point for the geodynamic models of formation of the crater core. It is not excluded that some authors derived their conclusions from the conception of the instantaneous ascent of the dome core by 7–9 km. This was reasonable, because such velocity followed from the numerical modeling of the process of *meteorite* crater formation (Melosh, 1989; Turtle and Melosh, 1996). However, the continuity and regular sequence of formation of various symplectite generations remained unexplored. As a consequence, the correct paths of the postimpact *P–T* evolution of metapelites from the core of the Vredefort dome were not derived.

There are at least two publications (Stevens *et al.*, 1997; Perchuk *et al.*, 2002) that presented evidence for the thermodynamic stability of undeformed porphyroblasts of *Grt*, *Opx*, and *Crd*[1] (without reaction structures), which were formed at regional metamorphism ~3 Ga ago (Hart, 1999). However, up to the present time, there is no comprehensive analysis of symplectite evolution up to the point of ultramylonite formation. Remind that Perchuk *et al.* (2002) suggested that the ultramylonites were formed continuously in the course of gradual relaxation of residual stresses accumulated in the rocks at their cooling and ascent toward the surface. During this ascent, orthopyroxene–cordierite symplectite substituted not only for primary garnet but also for pseudotachylites, which, in turn, resulted from the explosion (e.g., Schreyer, 1983; Gibson, 2002). However, the test of models of the sequence of symplectite formation in the Vredefort metapelites requires structural and analytical data on ultramylonite–symplectite relationships.

In 2001, we collected additional samples in the core of the Vredefort crater, and their purposeful examination revealed ultramylonites (Fig. 1) cutting symplectites in some of them. In this paper, we present the following data:

(1) the analysis of microscopic textural relationships between symplectites and ultramylonites;

(2) the results of a detailed microprobe investigation of minerals from these objects (Tables 1, 2); and

(3) the determination of the reason of the continuous decrease of *P–T* parameters at the final stage of upheaval of the central uplift of the Vredefort crater.

In our previous publication (Perchuk *et al.*, 2002), we considered in detail the geology of the Vredefort impact crater and discussed all the proposed ideas on the nature of its core. The repetition of these data in this paper would be superfluous. We proceed therefore directly to the presentation of factual material, characterization of the petrography of samples, and analysis of obtained data.

PETROGRAPHY AND MINERAL CHEMISTRY

Petrography

The rocks under investigation are typical *metapelites* of the Vredefort impact structure, which were repeatedly described by many authors (e.g., Perchuk *et al.*, 2002; Schreyer and Abraham, 1978; Stevens *et al.*, 1997; Gibson and Stevens, 1999; Gibson and Reimold, 2001). They show a massive structure and a porphyroblastic texture with the granoblastic fabric of the rock groundmass. The amounts of melanosome (*Grt* ± *Bt*) and leucosome (*Pl* + *Qtz* + *Kfs*) are approximately equal. Reaction structures are ubiquitous. They develop around anhedral grains of relict garnet (~5–7%) as *Crd* + *Opx* symplectites and outer plagioclase and/or hypersthene rims. Relatively thick, up to 100 μm and even more, hypersthene rims often develop at the direct contact of primary garnet with quartz grains (Fig. 2a). In this case, there is often no symplectite mantle. The grains of *Opx* and *Crd* from symplectites are no larger than a few micrometers in size (Fig. 2b). Tiny spinel grains (<1 μm) sometimes associate with orthopyroxene. Quartz inclusions in primary garnet are completely or partially replaced by orthopyroxene, which is compositionally identical to *Opx* from the coronas. In rare cases, garnet contains hercynite–quartz intergrowths (Stevens *et al.*, 1997). Aggregates and individual scales of biotite with explosion-related kink bands are rather common in the crystalline matrix of the rock. The grains of quartz and potassium feldspar (~50%) are isometric and anhedral. Plagioclase occurs in two generations. One of them (Pl_1) is represented by large anhedral crystals with exsolution perthites. It makes up the rock groundmass together with *Qtz* and *Kfs*. The plagioclase of the second generation (Pl_2) forms thin (up to 10 μm) rims separating symplectites from hypersthene coronas (Fig. 2a). Magnetite forms anhedral and, occasionally, subhedral grains.

Tiny stringers, lenses, and branching veinlets of *ultramylonite* impregnate the metapelite (Figs. 1a, 1b). Under an optical microscope, they show brown color and aphanitic or fine clastic textures. Their thickness is

[1] Mineral abbreviations: *Crd*, cordierite; *Grt*, garnet; *KFs*, potassium feldspar; *Opx*, orthopyroxene; *Pl*, plagioclase; and *Qtz*, quartz. Molar fractions of components in minerals: X_{Mg}^{Grt} = Mg/(Mg + Fe + Mn), X_{Ca}^{Grt} = Ca/(Ca + Mg + Fe + Mn), X_{Mg}^{Opx} = Mg/(Mg + Fe + Mn), X_{OK}^{Opx} = 0.5Al/(0.5Al + Fe + Mg), X_{Mg}^{Bt} = Mg/(Mg + Fe + Mn), and X_{Mg}^{Crd} = Mg/(Mg + Fe + Mn).

Table 1. Microprobe analyses along a profile through a garnet relict (*Grt*), symplectites (*Opx* + *Crd*) surrounding garnet, and *Opx* coronas in metapelite and minerals of ultramylonite (Figs. 1–3)

Component	Relict garnet surrounded by *Crd* + *Opx* symplectite in metapelite															
	59	58	57	56	55	54	53	60	52	30	31	32	33	34	96	73
	Grt	*Grt*	*Grt*	*Grt*	*Grt*	*Grt*	*Grt*	*Grt*	*Grt*	*Grt*	*Grt*	*Grt*	*Grt*	*Grt*	*Opx*	*Opx*
SiO_2	37.15	36.79	37.21	37.54	37.16	37.51	37.64	37.05	36.84	37.67	37.26	37.44	37.34	37.09	47.87	47.85
TiO_2	0.00	0.00	0.00	0.00	0.00	0.00	0.00	0.00	0.00	0.00	0.00	0.00	0.00	0.00	0.00	0.00
Al_2O_3	21.32	21.17	21.27	21.05	21.26	21.04	21	21.16	21.46	21.31	21.62	21.31	21.55	20.88	3.26	3.33
FeO	35.04	35.23	34.57	34.39	34.24	34.05	34.43	34.59	34.58	34.32	33.98	34.16	34.04	35.27	34.42	34.23
MnO	1.43	1.31	1.33	1.1	1.31	1.22	1.21	1.14	1.28	1.2	1.11	1.16	1.38	1.26	0.72	0.52
MgO	3.99	4.45	4.56	4.98	4.98	5.2	4.37	4.91	4.53	4.48	4.99	4.88	4.61	4.06	13.24	13.56
CaO	1.07	1.04	1.06	0.93	1.05	0.98	1.1	1.16	1.08	1.02	1.03	0.96	1.09	1.2	0.00	0.00
Cr_2O_3	0.00	0.00	0.00	0.00	0.00	0.00	0.00	0.00	0.00	0.00	0.00	0.00	0.00	0.00	0.00	0.00
Cation proportions																
Si	2.98	2.96	2.98	3	2.97	2.2	3.01	2.96	2.95	3.00	2.97	2.99	2.98	2.98	1.91	1.90
Ti	0.00	0.00	0.00	0.00	0.00	0.00	0.00	0.00	0.00	0.00	0.00	0.00	0.00	0.00	0.00	0.00
Al	2.02	2.00	2.01	1.98	2.00	1.98	1.98	2.00	2.03	2.00	3.20	2.00	2.03	1.98	0.15	0.16
Fe^{2+}	2.35	2.37	2.31	2.29	2.29	2.27	2.3	2.31	2.32	2.29	2.26	2.28	2.27	2.37	1.15	1.14
Mn	0.1	0.09	0.09	0.07	0.09	0.08	0.08	0.08	0.09	0.08	0.08	0.08	0.09	0.09	0.02	0.02
Mg	0.48	0.53	0.54	0.59	0.59	0.62	0.52	0.59	0.54	0.53	0.59	0.58	0.55	0.49	0.79	0.80
Ca	0.09	0.09	0.09	0.08	0.09	0.08	0.09	0.1	0.09	0.09	0.09	0.08	0.09	0.10	0.00	0.00
X_{Mg}	0.17	0.18	0.19	0.20	0.20	0.21	0.18	0.20	0.19	0.19	0.21	0.20	0.20	0.17	0.41	0.41
X_{OK}															0.038	0.039
Component	Symplectite in metapelite															
	71	69	67	65	63	61	50	48	46	35	37	39	74	72	70	68
	Opx	*Opx*	*Opx*	*Opx*	*Opx*	*Opx*	*Opx*	*Opx*	*Opx*	*Opx*	*Opx*	*Opx*	*Crd*	*Crd*	*Crd*	*Crd*
SiO_2	48.51	48.15	48.34	48.10	49.18	48.51	48.41	48.75	48.04	48.62	47.52	48.31	49.23	49.26	49.03	49.43
TiO_2	0.00	0.22	0.00	0.00	0.00	0.20	0.00	0.00	0.19	0.00	0.29	0.26	0.00	0.00	0.00	0.00
Al_2O_3	4.20	3.46	3.61	4.02	3.19	3.85	4.11	3.15	4.07	3.62	4.19	2.91	33.00	33.41	33.22	33.17
FeO	32.54	34.32	34.26	32.64	31.89	31.51	32.53	32.84	33.16	34.18	34.72	34.09	9.92	9.41	9.83	9.55
MnO	0.45	0.31	0.27	0.27	0.00	0.37	0.31	0.28	0.25	0.33	0.41	0.49	0.00	0.00	0.00	0.00
MgO	13.49	13.00	13.14	14.41	15.38	15.12	13.92	14.46	13.81	12.74	12.35	13.30	7.85	7.92	7.93	7.84
CaO	0.21	0.00	0.00	0.00	0.00	0.19	0.19	0.00	0.16	0.12	0.13	0.00	0.00	0.00	0.00	0.00
Cr_2O_3	0.00	0.25	0.25	0.00	0.00	0.25	0.25	0.26	0.33	0.25	0.33	0.00	0.00	0.00	0.00	0.00
Cation proportions																
Si	1.91	1.91	1.91	1.89	1.92	1.89	1.90	1.92	1.89	1.92	1.89	1.91	5.01	5.00	4.99	5.02
Ti	0.00	0.01	0.00	0.00	0.00	0.01	0.00	0.00	0.01	0.00	0.01	0.01	0.00	0.00	0.00	0.00
Al	0.20	0.16	0.17	0.19	0.15	0.18	0.19	0.15	0.19	0.17	0.20	0.14	3.96	4.00	3.99	3.97
Fe^{2+}	1.07	1.14	1.13	1.08	1.04	1.03	1.07	1.08	1.09	1.13	1.15	1.13	0.84	0.80	0.84	0.81
Mn	0.01	0.01	0.01	0.01	0.00	0.01	0.01	0.01	0.01	0.01	0.01	0.02	0.00	0.00	0.00	0.00
Mg	0.79	0.77	0.77	0.85	0.90	0.88	0.81	0.85	0.81	0.75	0.73	0.79	1.19	1.20	1.20	1.19
Ca	0.01	0.00	0.00	0.00	0.00	0.01	0.01	0.00	0.01	0.00	0.01	0.00	0.00	0.00	0.00	0.00
X_{Mg}	0.42	0.40	0.41	0.44	0.46	0.46	0.43	0.44	0.43	0.40	0.39	0.41	0.59	0.60	0.59	0.59
X_{OK}	0.0507	0.041	0.042	0.046	0.036	0.0444	0.048	0.036	0.047	0.043	0.05	0.034				

Table 1. (Contd.)

Component	Symplectite in metapelite									Coronas					
	66	64	62	51	49	47	36	38	40	76	75	42	43	44	45
	Crd	*Crd*	*Crd*	*Crd*	*Crd*	*Crd*	*Crd*	*Crd*	*Crd*	*Opx*	*Opx*	*Opx*	*Opx*	*Opx*	*Opx*
SiO_2	49.21	49.72	49.99	49.57	49.01	49.27	49.50	49.38	49.21	48.54	49.02	48.75	49.12	48.94	49.05
TiO_2	0.00	0.00	0.00	0.00	0.00	0.00	0.00	0.00	0.00	0.00	0.00	0.00	0.00	0.00	0.00
Al_2O_3	33.16	32.83	33.21	32.89	33.30	33.46	32.92	33.02	32.73	2.56	2.81	1.87	1.52	1.20	1.20
FeO	9.12	8.52	8.45	9.25	9.19	9.03	9.76	9.59	9.87	34.55	34.31	35.43	35.06	35.49	35.60
MnO	0.26	0.00	0.00	0.00	0.00	0.00	0.00	0.00	0.00	0.42	0.35	0.43	0.30	0.51	0.32
MgO	8.25	8.92	8.35	8.18	8.50	8.25	7.81	8.01	7.61	13.36	13.07	13.02	13.49	13.42	13.17
CaO	0.00	0.00	0.00	0.11	0.00	0.00	0.00	0.00	0.11	0.15	0.00	0.00	0.00	0.00	0.00
Cr_2O_3	0.00	0.00	0.00	0.00	0.00	0.00	0.00	0.00	0.00	0.00	0.32	0.19	0.00	0.00	0.00
Cation proportions															
Si	5.00	5.03	5.05	5.03	4.98	5.00	5.03	5.02	5.02	1.93	1.94	1.94	1.96	1.95	1.95
Ti	0.00	0.00	0.00	0.00	0.00	0.00	0.00	0.00	0.00	0.00	0.00	0.00	0.00	0.00	0.00
Al	3.97	3.91	3.95	3.93	3.99	4.00	3.95	3.96	3.93	0.12	0.13	0.09	0.07	0.06	0.08
Fe^{2+}	0.78	0.72	0.71	0.78	0.78	0.77	0.83	0.82	0.84	1.15	1.13	1.18	1.17	1.18	1.19
Mn	0.02	0.00	0.00	0.00	0.00	0.00	0.00	0.00	0.00	0.01	0.01	0.01	0.01	0.02	0.01
Mg	1.25	1.35	1.26	1.24	1.29	1.25	1.18	1.21	1.16	0.79	0.77	0.77	0.80	0.80	0.78
Ca	0.00	0.00	0.00	0.01	0.00	0.00	0.00	0.00	0.01	0.01	0.00	0.00	0.00	0.00	0.00
X_{Mg}	0.62	0.35	0.36	0.39	0.38	0.38	0.41	0.40	0.42	0.59	0.60	0.60	0.59	0.60	0.60
X_{OK}										0.03	0.033	0.022	0.018	0.015	0.0191

Component	Ultramylonite																
	90	89	88	87	86	83	94	81	79	77	76	75	85	82	80	78	95
	Opx	*Opx*	*Opx*	*Opx*	*Opx*	*Opx*	*Opx*	*Opx*	*Opx*	*Opx*	*Opx*	*Opx*	*Crd*	*Crd*	*Crd*	*Crd*	*Crd*
SiO_2	48.97	48.20	48.74	48.75	49.29	48.40	47.99	48.64	48.44	47.82	48.20	48.41	49.53	49.24	49.19	49.31	49.06
TiO_2	0.00	0.00	0.00	0.00	0.00	0.36	0.00	0.00	0.00	0.00	0.00	0.00	0.00	0.00	0.00	0.00	0.00
Al_2O_3	2.12	2.23	2.19	2.89	1.20	3.20	3.22	3.53	3.16	3.37	2.87	2.53	33.04	33.07	33.08	33.29	32.87
FeO	35.06	35.06	34.38	34.15	34.91	34.16	34.77	33.29	34.85	34.74	35.69	35.36	9.59	9.64	9.37	9.71	9.75
MnO	0.41	0.47	0.56	0.55	0.00	0.45	0.52	0.38	0.28	0.00	0.37	0.65	0.00	0.00	0.00	0.00	0.27
MgO	13.09	13.46	13.96	13.21	13.85	13.05	13.00	13.49	12.20	13.18	12.58	12.93	7.84	8.05	8.36	7.69	8.06
CaO	0.00	0.21	0.16	0.00	0.00	0.15	0.17	0.27	0.00	0.00	0.00	0.13	0.00	0.00	0.00	0.00	0.00
Cr_2O_3	0.00	0.00	0.00	0.00	0.00	0.23	0.25	0.00	0.27	0.29	0.00	0.00	0.00	0.00	0.00	0.00	0.00
Cation proportions																	
Si	1.95	1.92	1.94	1.93	1.96	1.91	1.91	1.92	1.92	1.90	1.92	1.93	5.03	5.01	5.00	5.01	5.00
Ti	0.00	0.00	0.00	0.00	0.00	0.01	0.00	0.00	0.00	0.00	0.00	0.00	0.00	0.00	0.00	0.00	0.00
Al	0.10	0.10	0.12	0.14	0.07	0.15	0.15	0.16	0.15	0.16	0.13	0.12	3.96	3.96	3.96	3.99	3.95
Fe^{2+}	1.17	1.17	1.14	1.13	1.16	1.13	1.16	1.10	1.16	1.16	1.19	1.18	0.81	0.82	0.80	0.83	0.83
Mn	0.01	0.02	0.02	0.02	0.00	0.02	0.02	0.01	0.01	0.00	0.01	0.02	0.00	0.00	0.00	0.00	0.02
Mg	0.78	0.80	0.78	0.78	0.82	0.77	0.77	0.79	0.75	0.78	0.75	0.77	1.19	1.22	1.27	1.17	1.22
Ca	0.00	0.01	0.01	0.00	0.00	0.01	0.01	0.01	0.00	0.00	0.00	0.01	0.00	0.00	0.00	0.00	0.00
X_{Mg}	0.40	0.41	0.41	0.41	0.41	0.40	0.40	0.42	0.39	0.40	0.39	0.39	0.59	0.60	0.61	0.59	0.60
X_{OK}	0.025	0.026	0.029	0.034	0.0175	0.038	0.038	0.042	0.037	0.039	0.034	0.03					

Table 2. Microprobe analyses of various plagioclase types from metapelite sample VF3-5

Component	Plagioclase in metapelite (Fig. 1)												Plagioclase in ultramylonite (Figs. 1, 2)		
	Matrix				Rims between *Crd* + *Opx* symplectite and *Opx* corona								Rim and matrix		
	26	111	112	114	3	5	16	21	41	115	116	119	20	25	84
SiO_2	59.47	61.54	60.29	59.79	54.55	56.66	55.15	57.93	58.76	58.10	57.24	58.72	59.07	59.55	59.20
Al_2O_3	25.36	24.22	24.94	25.08	28.48	26.92	27.77	26.37	26.10	26.26	26.54	25.74	25.51	25.58	25.68
FeO	0.28	0.00	0.00	0.43	0.48	0.64	0.74	0.48	0.44	0.47	0.69	0.48	1.00	0.51	0.53
CaO	7.46	6.10	6.92	7.07	10.52	9.13	10.59	8.21	8.02	8.30	8.50	7.94	7.31	7.14	7.56
Na_2O	7.28	7.99	7.67	7.49	5.65	6.37	5.49	6.74	6.54	6.87	6.92	7.00	7.00	7.23	7.03
K_2O	0.15	0.15	0.18	0.13	0.13	0.20	0.20	0.14	0.14	0.00	0.11	0.13	0.11	0.00	0.00
Cation formula															
Si	2.66	2.73	2.68	2.67	2.47	2.55	2.50	2.60	2.63	2.60	2.57	2.63	2.64	2.66	2.64
Al	1.33	1.27	1.31	1.32	1.52	1.43	1.48	1.39	1.37	1.39	1.41	1.36	1.35	1.34	1.35
Fe^{2+}	0.00	0.00	0.00	0.02	0.02	0.02	0.03	0.02	4.00	0.02	0.03	0.02	3.99	4.00	3.99
Ca	0.36	0.29	0.33	0.34	0.51	0.44	0.51	0.39	0.38	0.40	0.41	0.38	0.35	0.34	0.36
Na	0.63	0.69	0.66	0.65	0.50	0.56	0.48	0.59	0.57	0.60	0.60	0.61	0.61	0.62	0.61
K	0.01	0.01	0.01	0.01	0.01	0.01	0.01	0.01	0.01	0.00	0.01	0.01	0.01	0.00	0.00
X_{Ca}^{Pl}	0.36	0.30	0.33	0.34	0.51	0.44	0.52	0.40	0.40	0.40	0.40	0.39	0.37	0.35	0.37

Component	Plagioclase in ultramylonite (Figs. 1, 2)														
	Rim and matrix														
	92	93	97	25	27	39	46	49	54	93	98	100	101	104	105
SiO_2	59.43	60.11	57.94	57.78	58.40	57.75	59.74	59.48	59.55	58.56	58.34	58.79	58.79	59.60	59.65
Al_2O_3	25.13	25.10	25.87	25.63	25.72	24.90	24.93	25.24	24.70	25.80	25.84	25.59	24.85	24.92	24.96
FeO	0.36	0.53	1.97	0.88	0.65	2.06	0.68	0.61	0.42	0.84	0.79	0.62	0.83	0.85	0.35
CaO	7.57	7.18	7.26	7.98	7.59	7.43	6.68	7.15	6.84	7.17	7.36	7.40	6.99	6.80	6.87
Na_2O	7.41	6.85	6.95	7.31	7.26	7.36	7.87	7.34	8.25	7.48	7.16	7.38	8.05	7.54	7.84
K_2O	0.11	0.23	0.00	0.19	0.19	0.12	0.00	0.00	0.11	0.10	0.00	0.13	0.13	0.14	0.12
Cation formula															
Si	2.66	2.68	2.61	2.61	2.33	2.61	2.67	2.66	2.67	2.63	2.62	2.63	2.64	2.67	2.67
Al	1.32	1.32	1.37	1.36	1.36	1.33	1.31	1.33	1.30	1.36	1.37	1.35	1.32	1.32	1.31
Fe^{2+}	3.98	4.00	3.98	0.03	0.02	0.08	0.03	0.02	0.02	0.03	0.03	0.02	0.03	0.03	0.01
Ca	0.36	0.34	0.35	0.39	0.37	0.36	0.32	0.34	0.33	0.34	0.35	0.36	0.34	0.33	0.33
Na	0.64	0.59	0.61	0.64	0.63	0.65	0.68	0.64	0.72	0.65	0.67	0.64	0.70	0.66	0.68
K	0.01	0.01	0.00	0.01	0.01	0.01	0.00	0.00	0.01	0.01	0.01	0.01	0.01	0.01	0.01
X_{Ca}^{Pl}	0.36	0.37	0.37	0.38	0.37	0.36	0.32	0.35	0.31	0.35	0.34	0.36	0.32	0.33	0.33

no more than a few millimeters. The ultramylonites are mixtures of tiny mineral fragments, the largest of which are up to 900×400 μm in size. No traces of glass were found. By definition (Passchier and Trow, 1996), the presence of deformed minerals is one of the main characteristics of the mylonite. However, in the case of the Vredefort ultramylonites, many Fe–Mg mineral clusters experienced reaction transformations. Some of them are represented by newly formed cordierite–hypersthene symplectites. Their structure is very similar to that of the postimpact symplectites, which are widespread in the groundmass of the metapelite (Fig. 1b). Moreover, relicts of garnet are preserved in the central parts of relatively large fragments. They are

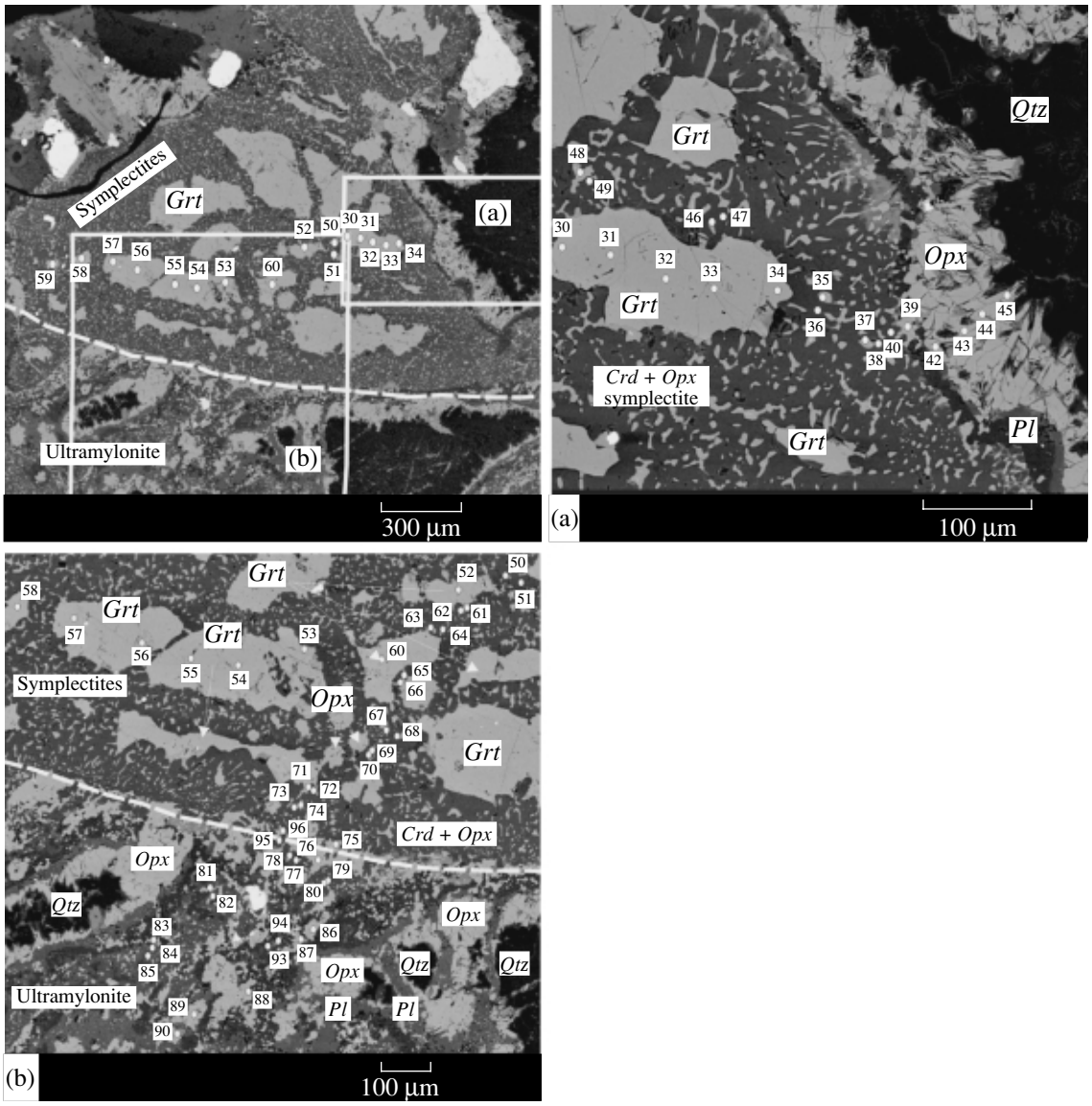

Fig. 2. Details of the boundary (white dashed line) of an ultramylonite veinlet in metapelite cutting a reaction structure at the contact of relict garnet with quartz in metapelite (Fig. 1). The reaction structure is composed of *Opx* + *Crd* symplectite surrounded by outer successive *Pl* and *Opx* mantles.

(a) *Opx* + *Crd* symplectite with *Opx* corona separating quartz (*Qtz*) from garnet (*Grt*). A thin plagioclase rim (*Pl*) develops at the inner part of the *Opx* corona. (b) A detail of the contact of symplectite and ultramylonite composed of tiny orthopyroxene fragments (light gray), cordierite, and plagioclase (dark gray). The boundaries between individual fragments are obscured. Fragments of *Qtz* and *Opx* rims are clearly seen in the ultramylonite. Back-scattered electron image. Numerals in the image correspond to analysis numbers in Tables 1 and 3.

surrounded by cordierite–hypersthene symplectites (Fig. 3), which formed in response to viscoelastic deformation. The boundaries between *Crd* + *Opx* symplectitic pseudomorphs after garnet are not clear in some cases.

In addition to reaction structures, the ultramylonite contains numerous quartz clusters. They are also surrounded by orthopyroxene mantles (Figs. 1, 3). They are completely undeformed and could either postdate the formation of the symplectites of the metapelite or be coeval with it. The quartz clusters are cemented by finely ground feldspar (*Pl* + *Kfs*) material (Fig. 3), which is almost indistinguishable from cordierite in back-scattered electron images. The plagioclase of the ultramylonite is compositionally similar to that of the metapelite groundmass (Table 2).

In addition to coronas, orthopyroxene occurs in the ultramylonite as rounded undeformed grains (Figs. 1, 3). Hypersthene rims often develop along the boundary of ultramylonite with quartz and metapelite (Figs. 1, 3).

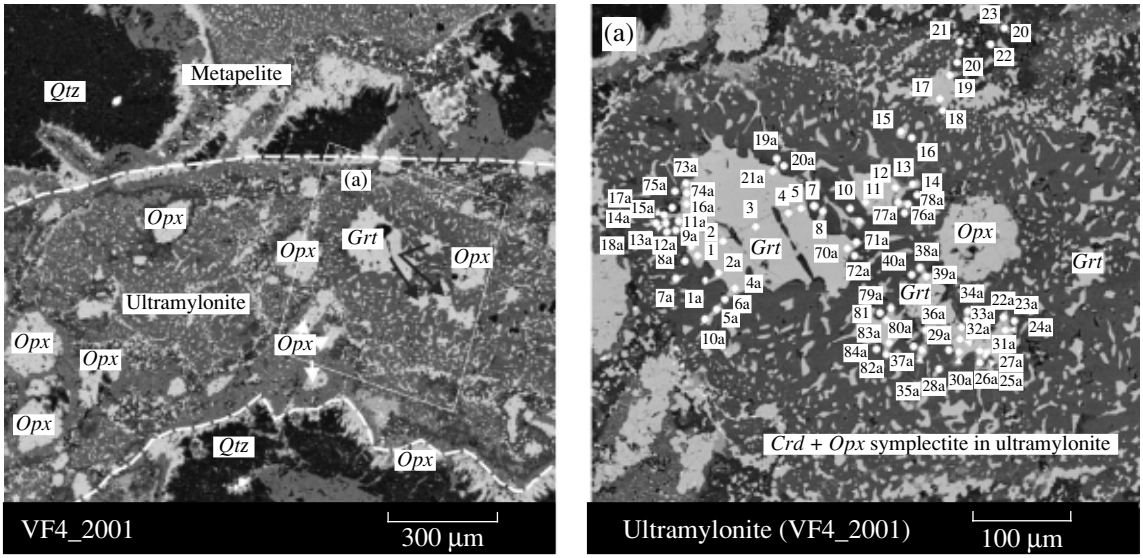

Fig. 3. A fragment of the ultramylonite shown in Fig. 1.

The boundaries are marked by dashed white lines. The ultramylonite contains abundant garnet fragments, which are replaced in most cases by *Opx* + *Crd* symplectites. Garnet (*Grt*) is rarely preserved as relicts in the symplectite. One of such fragments is contoured by the thin white line and is shown on the right image at higher magnification. It is seen that it is not deformed. Boundaries between individual fragments of symplectite in the ultramylonite are obliterated and vague, and *Opx* always develops at the contact with quartz. Rounded inclusions and aggregates of *Opx* occur around quartz clusters in the ultramylonite. They are cemented by very finely ground feldspathic material (*Pl* + *Kfs*). Back-scattered electron image. Numerals in the images correspond to analysis numbers in Table 4.

Mineral Chemistry

The compositions of minerals were investigated in the Laboratory of Electron Microscopy and Local Microanalysis of the Petrology Department, Moscow State University using a CamScan electron microscope equipped with a thoroughly calibrated Link system. The analyses were automatically recalculated to 100%, and their quality was checked by the correctness of the crystal chemical formula of analyzed mineral. The microprobe investigation included extensive systematic profiling of minerals in particular assemblages and reaction structures.

Metapelites. Profiles through relicts of primary garnet from the metapelite did not bring unexpected results: similar to previously analyzed samples (Perchuk *et al.*, 2002), X_{Mg}^{Grt} increases slightly from the central parts to the margins of grains. In the centers of grains, X_{Mg}^{Grt} is usually 0.2 and declines to 0.17–0.16 near the rims (Table 1, Fig. 4). Microprobe profiling through a complete reaction structure consisting of a hypersthene corona, a cordierite–hypersthene symplectite, and a relict of primary garnet (Figs. 1, 2) allowed us to evaluate changes in the compositions of all phases participating in the reaction *Grt* + *Qtz* ⇒ *Opx* + *Crd* (Figs. 1, 2; Table 1). In the grains of symplectitic orthopyroxene, which were formed at the expense of the quartz–garnet reaction, X_{Mg}^{Opx} declines from ~0.46 in the center to ~0.4 in the rim zone. The value X_{Mg}^{Opx} is almost constant in the coronas, 0.39–0.40 at X_{OK}^{Opx} = 0.02. A scatter in X_{OK}^{Opx} values within 0.05–0.03 is common in orthopyroxene from symplectite (Fig. 4, Table 1), and X_{OK}^{Opx} decreases to 0.02–0.03 in the coronas. The composition of plagioclase from the metapelite groundmass varies within X_{Ca}^{Pl} = 0.30–0.36 (Table 2). However, X_{Ca}^{Pl} is more variable in the plagioclase corona, from 0.52 to 0.39 (Table 2). Such high anorthite mole fractions in rim zones suggest plagioclase formation at the expense of the decomposition of a small amount of the grossular end-member of garnet at corona formation. Along the microprobe profile, near the contact with the ultramylonite (Fig. 2), X_{Mg}^{Opx} in symplectite from the metapelite decreases from 0.64 in the center of a porphyroblast to 0.58 in its margin (Fig. 4, Table 1).

Ultramylonites. A large (~600 μm) reaction structure (Fig. 3) was found among numerous tiny quartz, feldspars, and orthopyroxene clusters in the ultramylonite. Its central part is composed of several fragments of relict garnet surrounded by orthopyroxene–cordierite symplectites. A microprobe profile was recorded through this structure (Figs. 3a, 5; Table 3). It revealed main regularities in the changes of mineral compositions at the formation of the ultramylonite. It was found

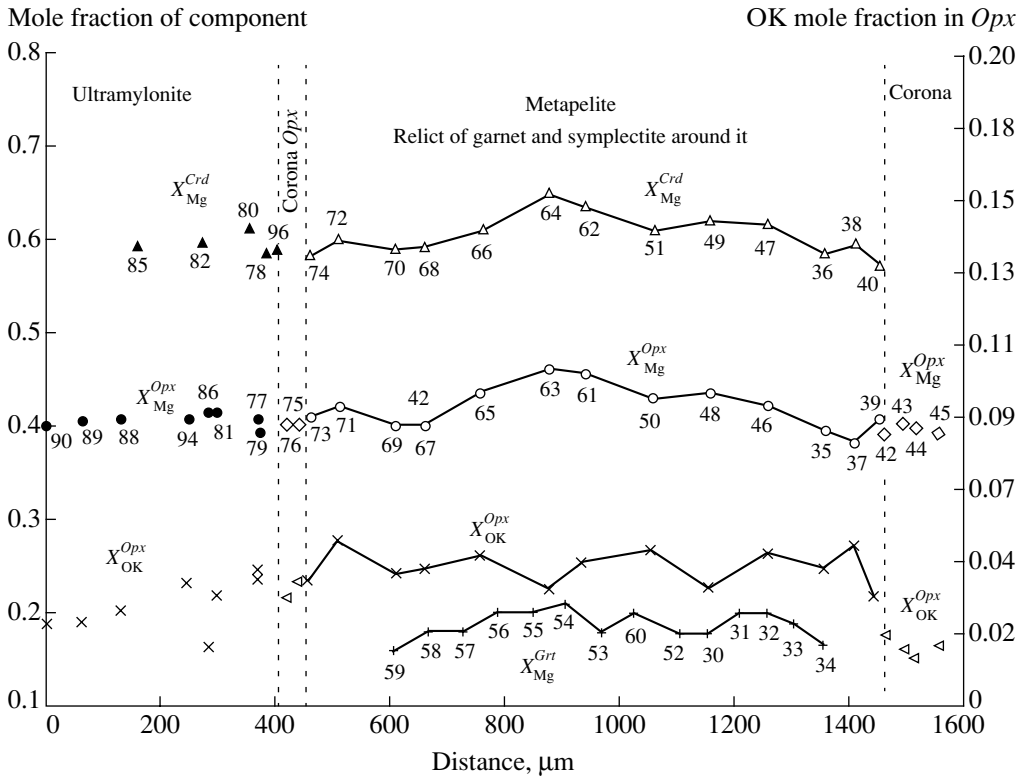

Fig. 4. Profiles of X^{Grt}_{Mg} in relict garnet and chemical zoning in the minerals of *Crd* + *Opx* symplectites and *Opx* corona around the symplectite (Fig. 2a, Table 1) from metapelite in contact with cutting ultramylonite (Figs. 1, 2a; Table 1).

that X^{Grt}_{Mg} declines from 0.18 in the central part of the relict to 0.15–0.14 near the margins of preserved fragments (Tables 1, 4; Figs. 3, 4). The values X^{Opx}_{Mg} are almost identical in relatively large grains and in the symplectite, 0.39–0.41, occasionally up to 0.45 (Tables 1, 4; Figs. 3, 5). The compositions of orthopyroxene from the coronas around garnet clusters in the ultramylonite and from the mantles surrounding quartz are practically identical: X^{Opx}_{Mg} = 0.39–0.41 and X^{Opx}_{OK} = 0.018–0.034 (Tables 1, 3; Figs. 3, 4). The compositions of tiny (up to 10 μm) orthopyroxene grains fall within the same ranges. The composition of cordierite from the symplectite changes insignificantly, X^{Crd}_{Mg} = 0.59–0.61 (Tables 1, 4; Figs. 3, 5). The anorthite mole fraction of plagioclase from the fine groundmass of the ultramylonite varies within X^{Pl}_{Ca} = 0.31–0.38 (Table 2).

DISCUSSION

As was mentioned above, the reaction structures from the metapelite and the ultramylonite cutting the metapelite are morphologically identical (compare back-scattered electron images in Figs. 2a and 4a). In both cases, the minerals of these reaction structures are undeformed and fairly identical in grain size (compare scale bars in Figs. 2a and 4a). However, there are important differences:

– cordierite, garnet, and orthopyroxene are richer in iron in the ultramylonite (Table 4), and the *P–T* parameters of mineral equilibria are lower (compare average values for two groups of symplectites in Table 4);

– the ultramylonites contain abundant tiny quartz and feldspar clusters, and in very rare instances, small garnet fragments with symplectite mantles were found;

– a hypersthene rim develops in the ultramylonite along the contact with the metapelite (Fig. 1).

Figure 3 shows how the outlines of a reaction structure in the ultramylonite are emphasized by plagioclase and orthopyroxene coronas surrounding the symplectite. These coronas cut reaction structures in the metapelites marking the latest stage in the history of Vredefort dome formation.

Perchuk *et al.* (2002) supposed that the reaction structures of the metapelites were the last crystallization processes in these rocks. However, in view of our investigation of the ultramylonite, this suggestion needs revision. The ultramylonite veinlets not only cut earlier symplectites (Fig. 1) but also contain iron richer minerals. Because of this, in this section, we must determine the conditions, place, and time of ultramylonite formation in the thermal and dynamic history of the Vredefort impact structure. This can be done through

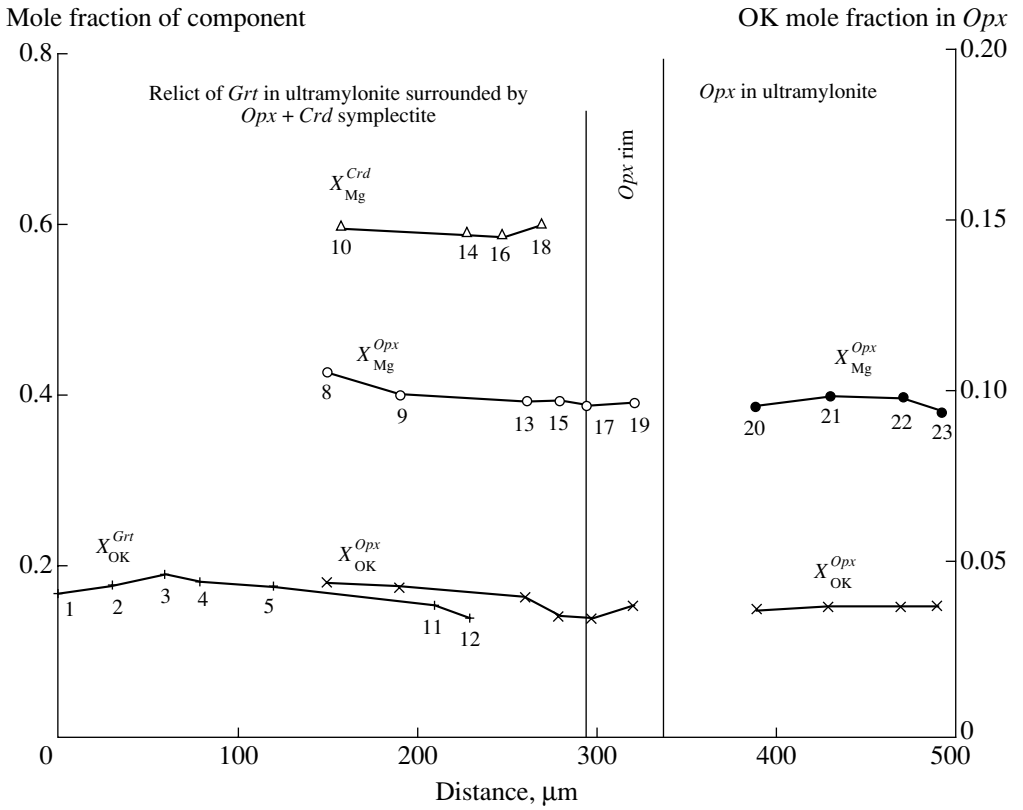

Fig. 5. A profile of the chemical zoning of minerals across the reaction structure *Grt* + *Qtz* ⇒ *Opx* + *Crd* in the ultramylonite shown in Fig. 3a. The analyses of minerals are given in Table 3.

the comparison of the previously derived *P–T* cooling path of rocks from the core of this structure (Perchuk *et al.*, 2002) with the *P–T* record in the local mineral equilibria of the ultramylonite. The solution of this problem may turn out to be fairly simple. For example, if the *P–T* parameters of ultramylonite formation are lower than the minimum *P–T* coordinates of the cooling paths of the symplectite groundmass in the granulites, this would imply that the ultramylonite was formed no earlier and no later than 2.023 Ga ago (Armstrong *et al.*, 1991).

Remind that there have been several attempts at deciphering the evolution of thermodynamic parameters for the core of the Vredefort dome and its framing on the basis of *P–T* paths (e.g., Gibson and Wallmach, 1995; Stevens *et al.*, 1997; Gibson and Reimold, 2001). Perchuk *et al.* (2002) reported recently a *P–T* path based on the systematic investigation of reactions with the participation of zonal minerals. Using this path, we were able to reconstruct the dynamic and thermal history of the Vredefort crater including symplectite formation. The method of its derivation (e.g., Perchuk *et al.*, 2002) is based on the detailed profiling of coexisting minerals including the reaction structures *Grt* + *Qtz* ⇒ *Opx* + *Crd* and *Grt* ⇒ *Crd* + *Sil* + *Qtz* from the granulites of the core of the Vredefort crater and hornfels of its framing, respectively. The profiling was usually accompanied by the systematic calculation of exchange and net-transfer reactions between phases (Perchuk, 1983), whose thermodynamic properties have been repeatedly published (e.g., Gerya and Perchuk, 2003; Perchuk *et al.*, 1996, 2000). This method was also applied for the estimation of the *P–T* parameters of formation of symplectites and ultramylonites from the metapelite under investigation.

Note also that Perchuk *et al.* (2002) presented the results of a detailed microprobe investigation of garnet, cordierite, and orthopyroxene porphyroblasts from the quartz–feldspar matrix of a weakly deformed metapelite collected in the granulite core of the Vredefort dome. On the basis of these data, a *P–T* path was derived for the metamorphic evolution of the rock before the explosion (Fig. 6, trend I), i.e., about 3.1 Ga ago (Hart, 1999). It was also demonstrated (Perchuk *et al.*, 2002) that granulite exhumation from a depth of ~15 km to ~8 km was not accompanied by symplectite formation. In contrast, owing to the shock activation of fluids, postimpact metamorphism resulted in the extensive symplectite development, which accompanied the relatively rapid ascent of the granulites over the whole path from ~8 km almost to the surface. Based on the available data, Perchuk *et al.* (2002) suggested that this ascent either did not occurred above ~3–4 km or was not recorded in mineral assemblages. The finding of ultramylonite and results of its investigation provide

Table 3. Microprobe analyses of minerals from the reaction structure *Grt* + *Qtz* ⟶ *Crd* + *Opx* of ultramylonite (Figs. 3a, 5)

Component	Relict *Grt*							*Crd* + *Opx* symplectite							
	1	2	3	4	5	11	12	8	9	13	15	10	14	16	18
	Grt	*Grt*	*Grt*	*Grt*	*Grt*	*Grt*	*Grt*	*Opx*	*Opx*	*Opx*	*Opx*	*Crd*	*Crd*	*Crd*	*Crd*
SiO_2	36.99	37.12	37.00	37.23	36.78	36.86	36.93	48.26	47.69	48.03	47.91	49.18	49.06	49.16	48.94
TiO_2	0.00	0.00	0.00	0.00	0.00	0.00	0.00	0.00	0.20	0.00	0.00	0.00	0.00	0.00	0.00
Al_2O_3	20.68	21.07	20.87	21.28	20.99	21.18	20.75	3.60	3.83	3.74	3.40	32.75	33.41	33.19	33.24
FeO	35.13	34.55	34.64	34.64	35.04	35.23	35.78	33.31	34.35	34.72	34.85	9.67	9.20	9.86	10.05
MnO	1.71	1.71	1.55	1.40	1.50	1.72	1.68	0.46	0.49	0.41	0.38	0.00	0.00	0.00	0.00
MgO	4.16	4.33	4.80	4.47	4.46	3.75	3.40	14.18	13.13	12.77	12.92	8.02	7.80	7.79	7.76
CaO	1.15	1.00	1.14	0.98	1.01	1.05	1.22	0.00	0.12	0.12	0.16	0.00	0.00	0.00	0.00
Cr_2O_3	0.19	0.22	0.00	0.00	0.22	0.21	0.24	0.20	0.20	0.21	0.33	0.00	0.00	0.00	0.00
Cation formula															
Si	2.98	2.98	2.97	2.98	2.96	2.97	2.98	1.90	1.89	1.90	1.90	5.01	4.99	5.00	4.99
Ti	0.00	0.00	0.00	0.00	0.00	0.00	0.00	0.00	0.01	0.00	0.00	0.00	0.00	0.00	0.00
Al	1.96	1.99	1.97	2.01	1.99	2.01	1.98	0.17	0.18	0.17	0.16	3.93	4.01	3.98	3.99
Fe^{2+}	2.37	2.32	2.32	2.32	2.36	2.37	2.42	1.10	1.14	1.15	1.57	0.82	0.83	0.84	0.86
Mn	0.12	0.12	0.11	0.09	0.10	0.12	0.11	0.02	0.02	0.01	0.13	0.00	0.00	0.00	0.00
Mg	0.50	0.52	0.57	0.53	0.54	0.45	0.41	0.83	0.77	0.75	0.76	1.22	1.18	1.18	1.18
Ca	0.10	0.09	0.10	0.08	0.09	0.09	0.11	0.00	0.00	0.01	0.01	0.00	0.00	0.00	0.00
Cr	0.01	0.01	0.00	0.00	0.01	0.01	0.02	0.01	0.00	0.01	0.01	0.00	0.00	0.00	0.00
X_{Mg}	0.17	0.18	0.19	0.18	0.18	0.15	0.14	0.43	0.40	0.39	0.31	0.60	0.59	0.58	0.58
X_{Ca}	0.03	0.03	0.03	0.03	0.03	0.03	0.03	0.00	0.00	0.00	0.00	0.00	0.00	0.00	0.00
X_{OK}	0.00	0.00	0.00	0.00	0.00	0.00	0.00	0.04	0.04	0.04	0.04	0.00	0.00	0.00	0.00

Component	*Opx* corona		Relict *Grt*												
	17	19	2a	4a	9a	11a	16a	21a	24a	27a	30a	31a	32a	36a	39a
	Opx	*Opx*	*Grt*	*Grt*	*Grt*	*Grt*	*Grt*	*Grt*	*Grt*	*Grt*	*Grt*	*Grt*	*Grt*	*Grt*	*Grt*
SiO_2	48.08	47.81	37.10	36.80	37.18	36.78	37.25	37.28	36.66	36.91	36.88	37.01	37.04	36.56	36.81
TiO_2	0.00	0.21	0.00	0.00	0.00	0.00	0.00	0.00	0.00	0.00	0.00	0.00	0.00	0.00	0.00
Al_2O_3	2.98	3.43	20.69	21.24	21.00	20.85	21.04	20.85	21.29	21.18	21.25	20.99	21.02	21.34	21.19
FeO	35.51	34.78	35.38	35.11	35.28	35.39	34.89	34.76	35.41	35.07	35.46	35.19	35.18	35.27	35.08
MnO	0.63	0.38	1.60	1.49	1.58	1.64	1.49	1.50	1.67	1.58	1.57	1.84	1.39	1.68	1.35
MgO	12.79	12.89	4.20	4.00	3.91	4.11	4.06	4.29	3.54	3.79	3.76	3.85	4.08	3.68	4.20
CaO	0.00	0.16	1.04	1.06	1.05	1.03	1.07	1.07	1.07	1.17	1.08	1.11	1.05	1.20	1.14
Cr_2O_3	0.00	0.33	0.00	0.29	0.00	0.21	0.20	0.25	0.37	0.30	0.00	0.00	0.23	0.27	0.22
Cation formula															
Si	1.91	1.90	2.99	2.96	2.99	2.96	2.99	2.99	2.96	2.97	2.97	2.98	2.98	2.95	2.96
Ti	0.00	0.01	0.00	0.00	0.00	0.00	0.00	0.00	0.00	0.00	0.00	0.00	0.00	0.00	0.00
Al	0.14	0.16	1.96	2.01	1.99	1.98	1.99	1.97	2.02	2.01	2.02	1.99	1.99	2.03	2.01
Fe^{2+}	1.18	1.15	2.38	2.36	2.37	2.39	2.34	2.33	2.39	2.36	2.39	2.37	2.36	2.38	2.36
Mn	0.02	0.01	0.11	0.10	0.11	0.11	0.10	0.10	0.11	0.11	0.11	0.13	0.09	0.11	0.09
Mg	0.76	0.76	0.50	0.48	0.47	0.49	0.49	0.51	0.43	0.45	0.45	0.46	0.49	0.44	0.50
Ca	0.00	0.01	0.09	0.09	0.09	0.09	0.09	0.09	0.09	0.10	0.09	0.10	0.09	0.10	0.10
Cr	0.00	0.01	0.00	0.02	0.00	0.01	0.01	0.02	0.02	0.02	0.00	0.00	0.01	0.02	0.01
X_{Mg}	0.39	0.40	0.17	0.16	0.16	0.17	0.17	0.17	0.15	0.16	0.15	0.16	0.17	0.15	0.17
X_{Ca}	0.00	0.00	0.03	0.03	0.03	0.03	0.03	0.03	0.03	0.03	0.03	0.03	0.03	0.03	0.03
X_{OK}	0.03	0.03	0.00	0.00	0.00	0.00	0.00	0.00	0.00	0.00	0.00	0.00	0.00	0.00	0.00

Table 3. (Contd.)

Component	*Crd* + *Opx* symplectite														
	1a	5a	7a	10a	13a	14a	17a	19a	22a	25a	28a	34a	35a	38a	6a
	Opx	*Opx*	*Opx*	*Opx*	*Opx*	*Opx*	*Opx*	*Opx*	*Opx*	*Opx*	*Opx*	*Opx*	*Opx*	*Opx*	*Crd*
SiO_2	48.57	48.90	47.93	48.00	48.53	48.07	47.96	47.81	47.60	47.92	48.42	48.39	48.23	48.47	49.50
TiO_2	0.24	0.00	0.00	0.00	0.00	0.00	0.00	0.19	0.00	0.19	0.00	0.00	0.00	0.00	0.00
Al_2O_3	3.42	3.34	3.41	3.43	3.59	3.37	3.46	3.54	3.94	3.68	3.23	3.51	3.59	3.72	33.36
FeO	33.00	34.06	34.85	34.83	33.24	34.71	34.84	34.32	35.23	33.79	34.61	33.70	33.95	32.94	8.97
MnO	0.51	0.48	0.40	0.55	0.33	0.46	0.51	0.36	0.30	0.40	0.48	0.41	0.39	0.45	0.00
MgO	13.86	13.21	13.05	12.85	14.05	13.38	12.79	13.44	12.66	13.88	13.07	13.71	13.61	14.06	8.18
CaO	0.18	0.00	0.11	0.13	0.00	0.00	0.16	0.00	0.00	0.13	0.00	0.00	0.00	0.16	0.00
Cr_2O_3	0.22	0.00	0.24	0.21	0.25	0.00	0.27	0.33	0.28	0.00	0.19	0.28	0.24	0.21	0.00
Cation formula															
Si	1.91	1.93	1.90	1.90	1.91	1.90	1.90	1.89	1.89	1.89	1.92	1.91	1.90	1.90	5.02
Ti	0.01	0.00	0.00	0.00	0.00	0.00	0.00	0.01	0.00	0.01	0.00	0.00	0.00	0.00	0.00
Al	0.16	0.16	0.16	0.16	0.17	0.16	0.16	0.17	0.18	0.17	0.15	0.16	0.17	0.17	3.98
Fe^{2+}	1.08	1.12	1.16	1.16	1.09	1.15	1.16	1.14	1.17	1.11	1.15	1.11	1.12	1.08	0.76
Mn	0.02	0.02	0.01	0.02	0.01	0.02	0.02	0.01	0.01	0.01	0.02	0.01	0.01	0.01	0.00
Mg	0.81	0.78	0.77	0.76	0.82	0.79	0.76	0.79	0.75	0.82	0.77	0.81	0.80	0.82	1.24
Ca	0.01	0.00	0.00	0.01	0.00	0.00	0.01	0.00	0.00	0.01	0.00	0.00	0.00	0.01	0.00
Cr	0.01	0.00	0.01	0.01	0.01	0.00	0.01	0.01	0.01	0.00	0.01	0.01	0.01	0.01	0.00
X_{Mg}	0.42	0.41	0.40	0.39	0.43	0.40	0.39	0.41	0.39	0.42	0.40	0.42	0.41	0.43	0.62
X_{Ca}	0.00	0.00	0.00	0.00	0.00	0.00	0.00	0.00	0.00	0.00	0.00	0.00	0.00	0.00	0.00
X_{OK}	0.04	0.04	0.04	0.04	0.04	0.04	0.04	0.04	0.05	0.04	0.04	0.04	0.04	0.04	0.00

Component	*Crd* + *Opx* symplectite												Small symplectites		
	6a	8a	12a	15a	18a	20a	23a	26a	29a	33a	37a	40a	21	22	29
	Crd	*Crd*	*Crd*	*Crd*	*Crd*	*Crd*	*Crd*	*Crd*	*Crd*	*Crd*	*Crd*	*Crd*	*Opx*	*Opx*	*Opx*
SiO_2	49.65	49.18	49.14	49.16	49.13	49.38	49.37	49.19	48.96	49.50	49.16	49.12	48.20	48.19	48.08
TiO_2	0.00	0.00	0.00	0.00	0.00	0.00	0.00	0.00	0.00	0.00	0.00	0.00	0.00	0.00	0.00
Al_2O_3	33.13	33.51	33.18	33.11	33.40	33.12	33.00	33.04	33.22	32.90	33.54	33.39	3.26	3.08	3.21
FeO	9.18	9.20	9.91	9.76	9.50	9.33	9.63	9.79	9.76	9.68	9.30	9.19	35.00	34.71	34.97
MnO	0.00	0.00	0.00	0.00	0.00	0.00	0.00	0.00	0.00	0.00	0.00	0.00	0.55	0.54	0.38
MgO	8.04	8.11	7.77	7.96	7.96	8.17	8.00	7.98	8.06	7.92	7.99	8.30	12.65	13.01	12.94
CaO	0.00	0.00	0.00	0.00	0.00	0.00	0.00	0.00	0.00	0.00	0.00	0.00	0.13	0.13	0.19
Cr_2O_3	0.00	0.00	0.00	0.00	0.00	0.00	0.00	0.00	0.00	0.00	0.00	0.00	0.21	0.34	0.23
Cation formula															
Si	5.03	4.99	5.00	5.00	4.99	5.01	5.02	5.01	4.98	5.03	4.99	4.99	1.91	1.91	1.91
Ti	0.00	0.00	0.00	0.00	0.00	0.00	0.00	0.00	0.00	0.00	0.00	0.00	0.00	0.00	0.00
Al	3.96	4.01	3.98	3.97	4.00	3.96	3.95	3.96	3.99	3.94	4.01	3.99	0.15	0.14	0.15
Fe^{2+}	0.78	0.78	0.84	0.83	0.81	0.79	0.82	0.83	0.83	0.82	0.79	0.78	1.16	1.15	1.16
Mn	0.00	0.00	0.00	0.00	0.00	0.00	0.00	0.00	0.00	0.00	0.00	0.00	0.02	0.02	0.01
Mg	1.21	1.23	1.18	1.21	1.21	1.24	1.21	1.21	1.22	1.20	1.21	1.26	0.75	0.77	0.77
Ca	0.00	0.00	0.00	0.00	0.00	0.00	0.00	0.00	0.00	0.00	0.00	0.00	0.01	0.01	0.01
Cr	0.00	0.00	0.00	0.00	0.00	0.00	0.00	0.00	0.00	0.00	0.00	0.00	0.01	0.01	0.01
X_{Mg}	0.61	0.61	0.58	0.59	0.60	0.61	0.60	0.59	0.60	0.59	0.60	0.62	0.39	0.40	0.39
X_{Ca}	0.00	0.00	0.00	0.00	0.00	0.00	0.00	0.00	0.00	0.00	0.00	0.00	0.00	0.00	0.00
X_{OK}	0.00	0.00	0.00	0.00	0.00	0.00	0.00	0.00	0.00	0.00	0.00	0.00	0.04	0.04	0.04

Table 4. *P–T* conditions of mineral equilibria in metapelite and ultramylonite at a water activity of 0.2

Grt			*Opx*			*Crd*		*T*, °C	*P*, kbar
Analysis no.	X_{Mg}	X_{Ca}	Analysis no.	X_{Mg}	X_{OK}	Analysis no.	X_{Mg}		
Crd + *Opx* symplectites around *Grt* in metapelite									
60	0.20	0.03	65	0.44	0.05	66	0.61	711	2.01
52	0.18	0.03	61	0.46	0.04	62	0.64	632	1.04
34	0.17	0.03	35	0.40	0.04	36	0.59	673	1.51
32	0.20	0.03	46	0.42	0.05	47	0.62	700	2.36
30	0.18	0.03	48	0.44	0.04	49	0.62	656	1.32
58	0.18	0.03	37	0.39	0.05	38	0.59	697	2.08
56	0.20	0.03	67	0.40	0.04	68	0.59	741	2.68
57	0.18	0.03	69	0.40	0.04	70	0.59	696	1.9
58	0.18	0.03	71	0.42	0.05	72	0.6	682	1.57
Average	0.19	0.03		0.42	0.04		0.61	688	1.83
Crd + *Opx* symplectites around *Grt* in ultramylonite									
5	0.18	0.03	8	0.43	0.04	7	0.61	669	1.45
11	0.15	0.04	9	0.4	0.04	10	0.6	618	0.74
12	0.14	0.04	13	0.39	0.04	14	0.59	606	0.46
17	0.17	0.03	15	0.4	0.04	16	0.59	673	1.51
70a	0.16	0.03	71a	0.43	0.04	72a	0.6	643	1.51
74a	0.17	0.03	73a	0.45	0.04	75a	0.59	669	0.69
80a	0.14	0.03	79a	0.41	0.05	81a	0.61	584	0.18
77a	0.15	0.03	76a	0.41	0.04	78a	0.58	638	0.50
83a	0.16	0.03	82a	0.41	0.05	84a	0.58	661	0.88
4a	0.16	0.03	5a	0.41	0.04	6a	0.62	624	1.57
11a	0.17	0.03	13a	0.43	0.04	12a	0.58	691	1.47
16a	0.17	0.03	17a	0.39	0.04	18a	0.60	671	2.22
24a	0.15	0.03	22a	0.39	0.05	23a	0.60	625	1.4
27a	0.16	0.03	25a	0.42	0.04	26a	0.59	657	1.28
30a	0.15	0.03	28a	0.40	0.04	29a	0.60	625	1.26
32a	0.17	0.03	34a	0.42	0.04	33a	0.59	680	1.67
36a	0.15	0.03	35a	0.41	0.04	37a	0.60	624	1.1
39a	0.17	0.03	38a	0.43	0.04	40a	0.62	644	1.61
Average	0.16	0.03		0.41	0.04		0.60	645	1.19

additional insight into this history. But previously, it is necessary to characterize the regime of water and carbon dioxide at the postimpact metamorphism of the Vredefort rocks.

According to theoretical and experimental investigations (e.g., Aranovich and Podlesskii, 1989), the position of isopleths in *P–T* diagrams for cordierite-bearing equilibria depends, to some extent, on the proportions of H_2O and CO_2 in the channels of the cordierite structure (~5 Å in diameter) formed by six-membered rings of Si–Al tetrahedra. The H_2O/CO_2 value of cordierite correlates with water content in fluid inclusions in coexisting quartz, sillimanite, and garnet (e.g., Perchuk, 2000). Schreyer (1983) noticed that the concentration of CO_2 in fluid inclusions from minerals of the Vredefort metapelites attained ~90%, which corresponds to $a^{fl}_{H_2O} = 0.2$. This value was used for the calculation of isopleths in the *P–T* diagram (Fig. 6, equilibrium *Grt* + *Qtz* = *Opx* + *Crd*) and estimation of *P–T* parameters using a combination of the *Crd–Grt* thermometer (Perchuk and Lavrent'eva, 1983) and the *Grt–Qtz–Opx–Crd* barometer (Gerya and Perchuk, 2003; Aranovich and Podlesskii, 1989).

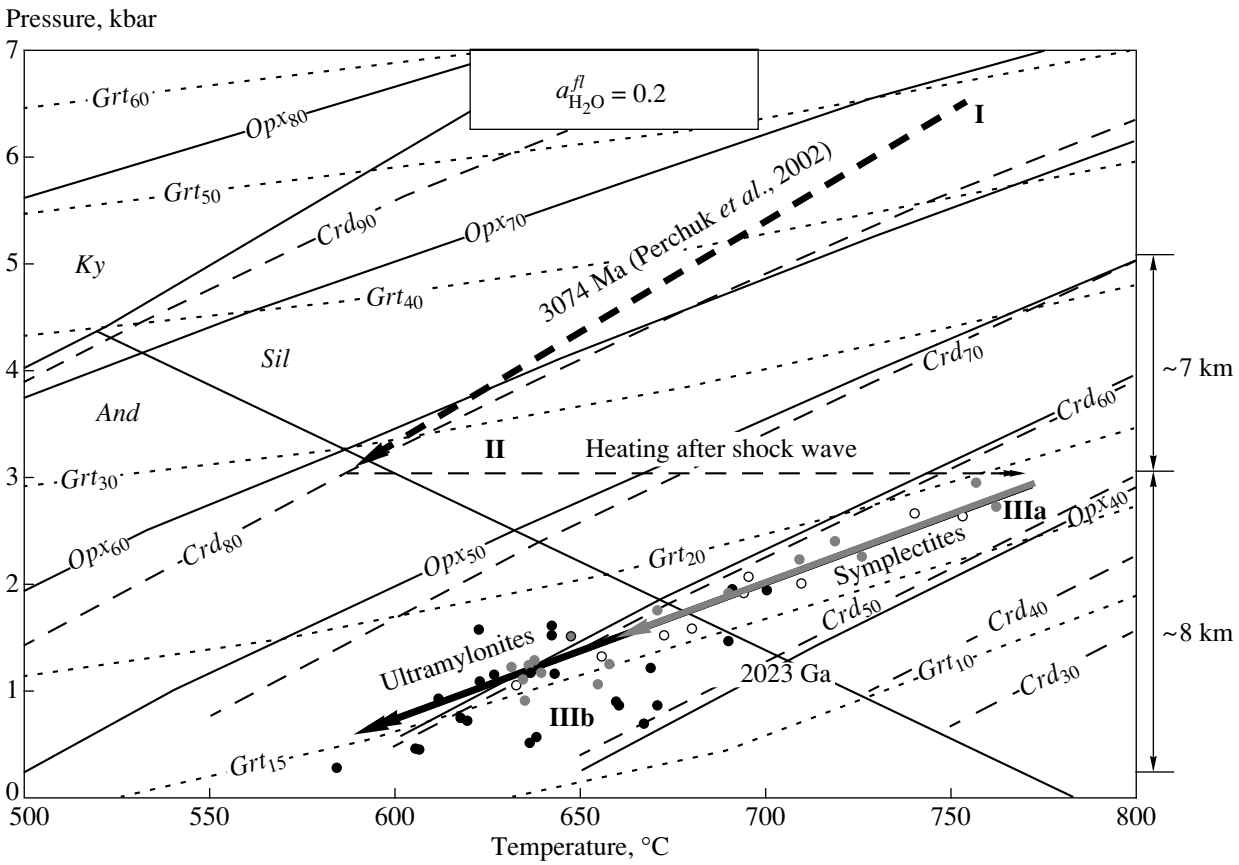

Fig. 6. *P–T* paths of formation of the reaction structures *Grt* + *Qtz* ⇒ *Opx* + *Crd* in metapelites from the core of the Vredefort crater. Part IIIa of trend III is recorded in symplectites from pseudotachylites and implies their formation after impact and heating (trend II) during the uplift of the crater core; part IIIb of trend III shows the conditions of the ultramylonite formation at the later stages of this uplift. These events probably occurred 2023 Ma ago (Armstrong *et al.*, 1991). The analyses are given in Tables 1, 3, and 4. For the sake of comparison, also shown are (I) the *P–T* path of exhumation of Archean granulites and points (gray circles) denoting the *P–T* paths of formation of symplectites in a number of other metapelite samples from the Vredefort impact structure (Perchuk *et al.*, 2002). All these data including isopleths of minerals in the equilibrium *Grt* + *Qtz* ⇒ *Opx* + *Crd* are calculated for a water activity in fluid of 0.2.

The postimpact *P–T* path in Fig. 6 is marked by white circles and denoted by the index III. The points of microprobe analysis are shown in Fig. 2a and in the upper part of Fig. 2b. The parameters of mineral coexistence in the symplectite are given in Table 4. The derived *P–T* path (Fig. 6) coincides almost exactly with the path that was reported for the same rocks by Perchuk *et al.* (2002). Being less steep than path I, it intersects, nonetheless, the garnet isopleths. This means that the reaction *Grt* + *Qtz* = *Opx* + *Crd* is shifted to the right reflecting relatively higher velocity of the ascent of the crater core in comparison with the rate of heat transfer into the wallrocks. Such a relationship of rates did not result in subisobaric cooling, which is common in deeper metamorphic levels (e.g., Perchuk *et al.*, 1996; Ellis, 1987; Sandiford and Powell, 1986).

Trend III extends from *P* = 3 kbar (~9 km) to a pressure of about 1 kbar (~3–4 km) and lower. The value *P* = 1 kbar in Fig. 6 is essentially identical to the average pressure for the ultramylonites (Table 4). The lowest estimates are only 460–500 bar and comparable with the accuracy of the geobarometer (e.g., Aranovich and Podlesskii, 1989).

In order to calculate the *P–T* parameters of mineral equilibria in the symplectite of ultramylonite, we used 54 microprobe analyses of touching cordierite, garnet, and orthopyroxene grains (Table 4). Clusters of relict garnet of varying size were preserved within the reaction structure that was studied by microprobe profiling (Fig. 3a). Their shape and distribution suggest that garnet and all other minerals were shattered before ultramylonite formation.

Black circles in Fig. 6 display the *P–T* path (IIIb) that was derived from the minerals of symplectite in the metapelite. Within the accuracy of the method, path IIIb is a termination of path IIIa (Fig. 2a and upper part of Fig. 2b). This trend suggests that after the explosion, the rocks of the crater core almost reached the surface ascending from a depth of 8–9 km. This estimate

was supported by many researchers (e.g., Stevens *et al.*, 1997; Gibson and Reimold, 2001).

Thus, the analysis of the *P–T* paths (Fig. 6) suggests that the ultramylonite was formed at the latest stage of ascent of the granulite core of the crater, i.e., very close to the surface. The region of their formation lies beyond the water-saturated granite minimum, which suggests that all transformations in the rocks occurred in the solid state (dynamometamorphism). The only mechanism of their formation was the relaxation of residual stresses related to the relatively rapid upheaval of the dome.

CONCLUSION

In addition to numerous tiny clusters (fragments) of quartz, feldspars, orthopyroxene, and garnet, the ultramylonites bear *Grt + Qtz* ⇒ *Opx + Crd* reaction structures similar to those often observed in the metapelites of the Vredefort crater. *Opx + Crd* symplectites always develop around garnet clusters, but distinct hypersthene coronas are not ubiquitous. Geobarometric measurements demonstrated that the ultramylonites were formed at lower *P–T* parameters in comparison with any other reaction structures of the granulite. Their *P–T* path of metamorphic evolution completes the path of symplectite groundmass and goes below the water-saturated granite minimum. This implies that the ultramylonites resulted from the relaxation of residual stresses accumulated during the ascent of the central uplift of the crater. Thus, this investigation has led us to a single conclusion: the ultramylonites were formed near the surface at the final stage of the dynamic and thermal history of the Vredefort impact structure 2.023 Ga ago. This provides additional support to our previous model of the formation of the Vredefort dome (Perchuk *et al.*, 2002) and puts an end to the discussion of many years on the relationships between the ultramylonites (thin pseudotachylite veinlets in the terminology of Schreyer, 1983) and their host granulite metapelites.

ACKNOWLEDGMENTS

The authors thank M.S. Brink, D.A. Varlamov, Kimikatsu Hisada, and Eiko Hisada for the assistance in collecting samples, and W. Schreyer for the heated discussions on the role of pseudotachylites in the interpretation of the history of the Vredefort impact crater. This study was carried out in the framework of the scientific collaboration of the Petrology Department of Moscow State University, the Institute of Experimental Mineralogy of the Russian Academy of Sciences, and the Department of Geology of Rand Afrikaans University and was financially supported by the RSA NRF and Russian Foundation for Basic Research, project nos. 00-05-64939 (TVG), 02-05-64025 (LLP), and 00-15-98519 (Leading Russian Scientific Schools, cosupervisor L.L. Perchuk).

REFERENCES

Allen, A.R., Mechanism of Friction Fusion in Fault Zones, *J. Structural Geol.*, 1979, vol. 1, no. 3, pp. 231–243.

Aranovich, L.Ya. and Podlesskii, K.K., Geothermobarometry of High-Grade Metapelites: Simultaneously Operating Reactions, in *Evolution of Metamorphic Belts*, Daly, S., Yardley, B.W.D. and Cliff, B., Eds., *Geol. Soc. London Spec. Publ.*, 1989, pp. 41–65.

Armstrong, R.A., Compston, W., Retief, E.A., *et al.*, Zircon Ion Microprobe Studies Bearing on the Age and Evolution of the Witwatersrand Basin, *Precambrian Res.*, 1991, vol. 53, pp. 243–256.

Ellis, D.J., Origin and Evolution of Granulites in Normal and Thickened Crust, *Geology*, 1987, vol. 15, pp. 167–170.

Gerya, T.V. and Perchuk, L.L., Ascent of Granulite Diapirs: I. Numerical Model, in *Eksperimental'naya mineralogiya na rubezhe stoletii* (Experimental Mineralogy at the Turn of Centuries), Moscow: Nauka, 2003 (in press).

Gibson, R.L. and Reimold, W.U., The Vredefort Impact Structure, South Africa. The Scientific Evidence and Two-Day Excursion Guide, *Council Geosci. of South Africa*, 2001, Memoir 92.

Gibson, R.L. and Stevens, G., Regional Metamorphism Due to Anorogenic Intracratonic Magmatism, in *What Drives Metamorphism and Metamorphic Reactions?*, Treloar, P.J. and O'Brien, P.J., Eds., *Geol. Soc. London Spec. Publ.*, 1998, vol. 138, pp. 121–135.

Gibson, R.L. and Wallmach, T., Low Pressure–High Temperature Metamorphism in the Vredefort Dome, South Africa: Anticlock-Wise *P–T* Path Followed by Rapid Decompression, *Geol. J.*, 1995, vol. 30, pp. 319–331.

Gibson, R.L., Impact-Induced Melting in Archean Granulites in the Vredefort Dome, South Africa. I: Anatexis of Metapelitic Granulites, *J. Metamorph. Geol.*, vol. 20, pp. 57–70.

Gibson, R.L., Reimold, W.U., and Stevens, G., Thermal-Metamorphic Signature of an Impact Event in the Vredefort Dome, South Africa, *Geology*, 1998, vol. 26, pp. 787–790.

Gibson, R.L., Reimold, W.U., and Wallmach, T., Origin of Pseudotachylite in the Lower Witwatersrand Supergroup, Vredefort Dome (South Africa): Constraints from Metamorphic Studies, *Tectonophysics*, 1997, vol. 283, pp. 241–262.

Hart, R.J., Vredefort Dome Field Guide, *Kaapvaal Craton Workshop, 6–9 April 1999*, Univ. Witwatersrand, Schonland Res. Center, 1999.

Korzhinskii, D.S., *Izbrannye trudy: Petrologiya metamorfizma* (Selected Works: Petrology of Metamorphism), Moscow: Nauka, 1999.

Martini, J.E.J., The Metamorphic History of the Vredefort Dome at Approximately 2 Ga as Revealed by Coesite–Stishovite-Bearing Pseudotachylites, *J. Metamorph. Geol.*, 1992, vol. 10, pp. 517–527.

Melosh, H.J., *Impact Cratering—A Geological Process*, New York: Oxford Univ. Press, 1989.

Passchier, C.W. and Trow, R.A., *Microtectonics*, Berlin: Springer, 1996.

Perchuk, L.L. and Lavrent'eva, I.V., Experimental Investigation of Exchange Equilibria in the System Cordierite–Garnet–Biotite, in *Advances in Physical Geochemistry*, New York: Springer, 1983, pp. 199–239.

Perchuk, L.L., Derivation of a Thermodynamically Consistent System of Geothermometers and Geobarometers for

Metamorphic and Magmatic Rocks, in *Progress in Metamorphic and Magmatic Petrology*, Perchuk, L.L., Ed., Cambridge Univ. Press, 1990, pp. 93–112.

Perchuk, L.L., Gerya, T.V., Van Reenen, D.D., *et al.*, Comparable Petrology and Metamorphic Evolution of the Limpopo (South Africa) and Lapland (Fennoscandia) High-Grade Terrains, *Mineral. Petrol.*, 2000, vol. 69, pp. 69–107.

Perchuk, L.L., Gerya, T.V., van Rinen, D.D., *et al.*, The Limpopo Metamorphic Complex, South Africa: The Regime of Decompression and Isobaric Cooling of Granulites and Related Rocks in the Kaapvaal Craton, *Petrologiya*, 1996, no. 6, pp. 619–648.

Perchuk, L.L., Podladchikov, Yu.Yu., and Polyakov, A.N., Geodynamic Modeling of Some Metamorphic Processes, *J. Metamorph. Geol.*, 1992, vol. 10, pp. 311–318.

Perchuk, L.L., *P–T* Fluid Regimes of Metamorphism and Related Magmatism with Specific Reference to the Baikal Lake Granulites, in *Evolution of Metamorphic Belts*, Daly, S., Yardley, D.W.D., and Cliff, B., Eds., *Geol. Soc. London Spec. Publ.*, 1989, vol. 42, pp. 275–291.

Perchuk, L.L., The Thermodynamic Aspect of Polymetamorphism, in *Metamorficheskaya zonal'nost' i polimetamorficheskie kompleksy* (Metamorphic Zoning and Polymetamorphic Complexes), Moscow: Nauka, 1983, pp. 134–140.

Perchuk, L.L., Tokarev, D.A., van Rinen, D.D., *et al.*, The Dynamic and Thermal History of the Impact Structure in the Kaapvaal Craton, South Africa, *Petrologiya*, vol. 10, no. 5, pp. 451–492.

Ramberg, H., *Gravity, Deformation and the Earth Crust*, London: Academic, 1967. Translated under the title *Sila tyazhesti i deformatsii v zemnoi kore*, Moscow: Nedra, 1985.

Sandiford, M. and Powell, R., Deep Crustal Metamorphism during Continental Extension: Ancient and Modern Examples, *Earth Planet. Sci. Lett.*, 1986, vol. 79, pp. 151–158.

Sazonova, L.V. and Korotaeva, N.N., The Genesis and Formation Parameters of Ultramylonites and Pseudotachylytes in the Central Uplift of the Puchezh–Katun' Astrobleme, *Vestn. Mosk. Univ., Ser. 4: Geol.*, 1995, no. 1, pp. 74–81.

Schreyer, W. and Abraham, K., Symplectitic Cordierite–Orthopyroxene–Garnet Assemblages as Products of Contact Metamorphism of Preexisting Basement Granulites in the Vredefort Structure, South Africa, *Contrib. Mineral. Petrol.*, 1978, vol. 68, pp. 3–62.

Schreyer, W., Metamorphism and Fluid Inclusions in the Basement of the Vredefort Dome, South Africa: Guidelines to the Origin of the Structure, *J. Petrol.*, 1983, vol. 24, pp. 26–47.

Shand, S.I., The Pseudotachylyte of Parys (Orange Free State) and Its Relation to "Trap-Shotten Gneiss" and "Flinty Crush-Rock," *Quart. J. Geol. Soc.*, 1916, no. 72, pp. 198–217.

Stevens, G., Gibson, R.L., and Droop, G.T.R., Mid-Crustal Granulite Facies Metamorphism in the Central Kaapvaal Craton: The Bushveld Complex Connection, *Precambrian Res.*, 1997, vol. 82, pp. 113–132.

Stow, G.M., *Report of the Geological Survey of the Orange Free State from 18 April to 17 December, 1879*, Bloemfontein, 1879, pp. 18–24.

Turtle, E.PP. and Melosh, H.J., Finite Element Modeling of the Vredefort Impact Structure with Implications for the Collapse and Modification Stage of Large Crater Formation, Lunar and Planet Science 1996, Abstract of Papers *27th Lunar and Planet Science Conference, March 18–22, Houston*, 1996, vol. 27, pp. 1347–1348.

Wise, D.U., Dunn, D.E., Englder, J.T., *et al.*, Fault-Related Rocks: Suggestion for Terminology, *Geology*, 1984, vol. 12, pp. 381–394.